RSC Advances

PAPER

View Article Online
View Journal | View Issue

Check for updates

Cite this: *RSC Adv.*, 2021, **11**, 6346

From cow manure to bioactive carbon dots: a light-up probe for bioimaging investigations, glucose detection and potential immunotherapy agent for melanoma skin cancer†

Frederico Hillesheim Horst,[a] Carime Vitória da Silva Rodrigues,*[b] Pedro Henrique Pimenta Rocha Carvalho,[c] Amanda Monteiro Leite,[b] Ricardo Bentes Azevedo,[a] Brenno A. D. Neto,[c] José Raimundo Corrêa,[c] Mônica Pereira Garcia,[a] Saud Alotaibi,[d] Mohamed Henini,[d] Sacha Braun Chaves[a] and Marcelo Oliveira Rodrigues[bd]

Received 27th December 2020
Accepted 18th January 2021

DOI: 10.1039/d0ra10859f

rsc.li/rsc-advances

Bioactive carbon dots (**C-dots**) with *ca.* 4 nm were successfully produced with singular photophysical properties, low-toxicity and interesting immunological response. The optical properties of the **C-dots** were investigated and the "light-up" behaviour enabled them to be explored in glucose detection and bioimaging experiments (mitochondrial selective probe). **C-dots** were not selective to the tumour region and several fluorescent spots were visualized spread on animal bodies. The histology investigations showed that cancer-bearing mice treated with **C-dots** presented a large number of regions with necrosis and inflammatory infiltrates, which were not identified for cancer-bearing mice without the treatment. These results suggested that **C-dots** have the potential to be explored as an immune therapy agent for melanoma skin cancer.

Open Access Article. Published on 03 ferraghju 2021. Downloaded on 30/07/2025 8:35:33.
This article is licensed under a Creative Commons Attribution-NonCommercial 3.0 Unported Licence.

Introduction

Cancer is a general term for a group of diseases characterized by the disorderly spread and growth of defective cells. It can be detected in any part of the body and its mortality rate is globally increasing. Those diseases are expected to be the major cause of death in the 21st century.

Nanotechnology has been an important allied on fighting cancer.[1,2] The versatility of nanomaterials in cancer therapy has contributed for recent innovations in drug delivery systems and enabled the creation of new therapeutic agents based on particle surface functionalization with molecules and biomolecules (nucleic acid strands, peptides, proteins or antibodies).[3,4] These sophisticated multifunctional nanosystems can contribute to more precise diagnostics and less invasive treatments.

It is well-known that compounds containing boronic acid-groups can be widely used in the diagnostic and treatment of different pathologies.[5–8] Several reports have described these compounds as selective taggants of glycoproteins, inhibitors of virus and bacterias, immunopotentiators and/or imunosensitization agents of tumour cells.[9,10] Boronic acid group can form highly-stable cyclic esters with *cis*-1,2 and 1,3-Lewis base molecules (alcohol and amine) in biological media. This important characteristic enabled the development of specific enzyme inhibitors that can be used for Alzheimer's disease and cancer treatments.[11–13] For instance, the peptidylboronic antineoplastic agent Bortezomib has been used in cancer treatment since 2003.[14]

Phenylboronic acid (PBA) belongs to a class of organic ligands that are widely employed for molecular recognition. Reports have indicated that PBA can target and reduce the proliferation process of prostate and breast cancer cells.[15,16] *In vivo* investigations demonstrated the effectiveness of nanoparticles coated with boronic groups in prolonging the survival time of cancer-bearing mice and reducing tumour growth.[16,17] PBA derivatives can also mimic the recognition properties of the lectins for tagging sugar fragments on cell surface.[14] Liu and coworkers produced a PBA-containing polymer which can reversibly capture and release cancer cells depending on the pH and glucose concentration.[18] In another example, Deshayes and coworkers have shown that a nanocarrier containing PBA

[a]*Department of Genetics and Morphology, Institute of Biological Sciences, Campus Universitário Darcy Ribeiro, Brasília-DF, CEP 70910900, Brazil*

[b]*LIMA-Laboratório de Inorgânica e Materiais, University of Brasilia, Campus Universitário Darcy Ribeiro, Brasília-DF, CEP 70910900, Brazil. E-mail: carime.v.rodrigues@gmail.com*

[c]*Laboratory of Medicinal & Technological Chemistry, University of Brasilia, Campus Universitário Darcy Ribeiro, Brasília-DF, CEP 70910900, Brazil*

[d]*School of Physics and Astronomy, Nottingham University, Nottingham, NG72RD, UK*

† Electronic supplementary information (ESI) available: All experimental procedures and experimental data. See DOI: 10.1039/d0ra10859f

© 2021 The Author(s). Published by the Royal Society of Chemistry

Open Access Article. Published on 03 ferraghju 2021. Downloaded on 30/07/2025 8:35:33.
This article is licensed under a Creative Commons Attribution-NonCommercial 3.0 Unported Licence.

fragments and a parent complex of the anticancer drug oxaliplatin was able to reduce the growth rate of both orthotopic and lung metastasis models of melanoma *in vivo*.[13]

Recent studies have demonstrated that malignant cell transformation, tumour growth, metastasis and the pessimistic prognosis in some cancer patients have been directly associated with the hypersialylation of the plasmatic cell membrane.[19] Aberrant Sialic Acid (SA) overexpression protects the cancer cell against immune recognition and eradication, and facilitates migration and tissue invasion.[20] Galvan and co-workers have confirmed the correlation between the SA levels and the progression of malignant melanoma in 25 patients.[21] In accordance with this study, patients in advanced melanoma stages presented high levels of SA in comparison with those in the early stage. Antibody and lectins have been widely explored for profiling the hyperexpression of SA onto the cell surface, while other strategies appeal for recombinant and SA-bind proteins for detecting anomalies in sialy glycans on cells and tissues.[22] However, these biomolecule-based strategies, that normally are expensive and very time-consuming, require complicated methods and costly equipments.

Cancer treatment based on boronic acid containing molecules have been widely reported.[17] For instance, Plopper and co-workers demonstrated that PBA is selective and effective to reduce viability and migration of prostate and breast cancer cells.[23] In another *in vitro* and *in vivo* investigation, PBA inhibited 57% of endocarcinoma 4T1 growth after intraperitoneal administration in mice.[12] Nagasaki and co-workers reported a PBA-decorated polymeric nanoparticle that is effective against a B16 melanoma-bearing mice model.[24]

Among the nanomaterials used against cancer, a new class of material has recently emerged and is showing promising results, that is, the carbon dots (**C-dots**).[25–27] **C-dots** are spheroidal nanoparticles with sizes typically smaller than 10 nm, composed by a graphitic core and covered by an amorphous carbonaceous edge.[25,28] **C-dots** modified with PBA moieties can present outstanding selectivity for glycoproteins and antineoplastic properties that make them interesting nanoplatforms for the development of theragnostic tools.[29,30] Based on our interest in the development of optical probes with more selective properties and cancer treatment, this work presents the synthesis, characterization and biological investigation of a simple luminescent platform based on surface-modified **C-dots** with PBA (**PBAC-dots**). We also report the exploration of **PBAC-dots** as a light-up probe for saccharide, bioimaging agent and a potential immunotherapy agent for melanoma skin cancer.

Results and discussion

The production and passivation of **C-dots** were performed in accordance with our previous work using cow manure or glucose as the carbon sources.[31] 4-Formylphenylboronic acid (4-FPBA) was covalently bonded to primary amines of the passivated **C-dots** by Schiff base formation followed a reduction with sodium borohydride (see Scheme 1).

Fig. 1 shows high-resolution HRTEM images and particle size distributions acquired of the **PBAC-dots**. The spheroidal **PBAC-dots** are well-dispersed and presented narrow size distribution ranging from 2–6 nm with average diameter of 4.2 nm ± 0.032 nm. Fig. 1(a) exhibits a representative HRTEM image of an individual particle. **PBAC-dots** presents high crystalline structure with lattice parameter of 2.2 Å, which agrees well with [100] lattice spacing of graphene along the [001] diffraction plane.[32]

The XPS spectrum of the **PBAC-dots** (Fig. 1(c)) clearly displays five elements, O, N, C, S and B, and their contents are 39.10%, 4.11%, 48.00%, 3.45% and 5.42%, respectively. The presence of boron onto **PBAC-dots** surface indicates that PBA moieties were successfully introduced in the synthesis process. The high-resolution XPS spectra are available in ESI.† C 1s spectrum presents three peaks at 289.4, 286.6 and 285.3 eV which can be assigned to the C=O, C=C and C–C bonds, respectively (Fig. S1(a)†). Fig. S1(b)† is the O 1s line that shows peaks at 532.4, 533.62 and 535.6 eV related to –C=O, C–O and

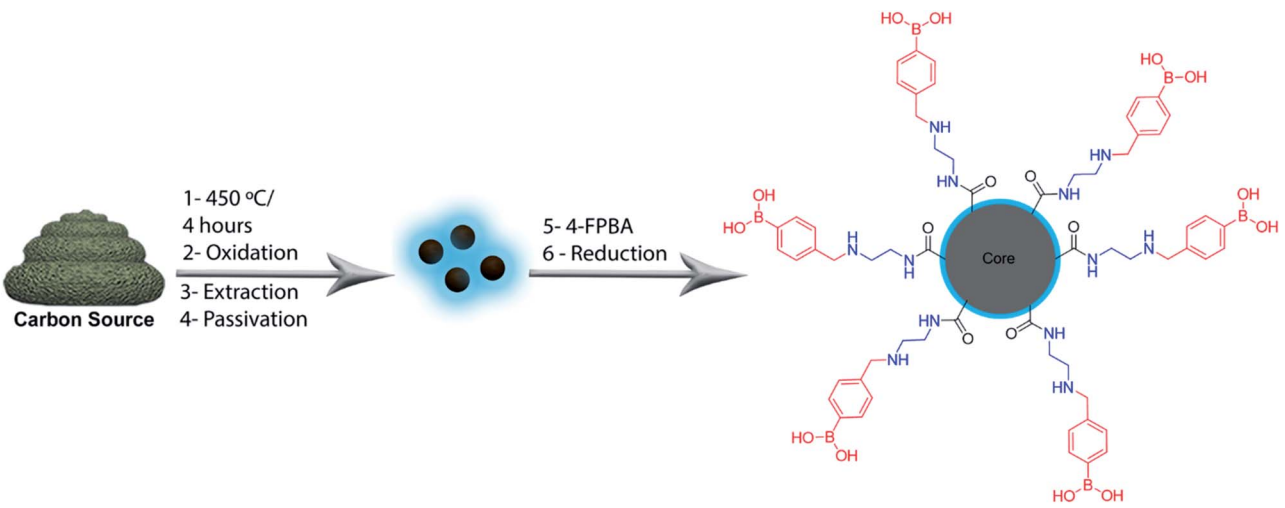

Scheme 1 Schematic approach adopted for production of PBAC-dots.

Open Access Article. Published on 03 ferraghju 2021. Downloaded on 30/07/2025 8:35:33.
This article is licensed under a Creative Commons Attribution-NonCommercial 3.0 Unported Licence.

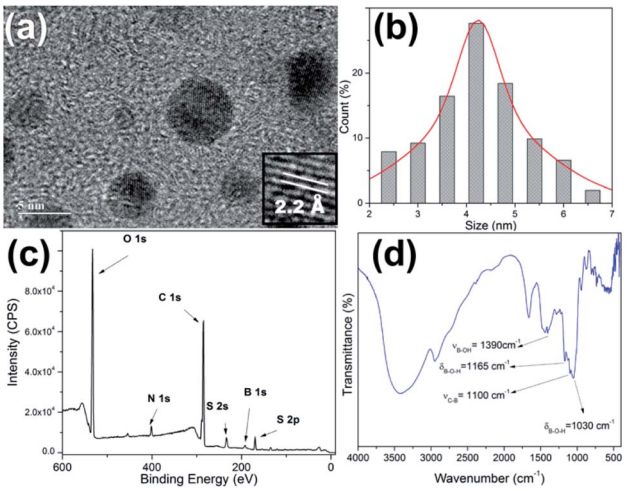

Fig. 1 (a) HRTEM image of the **PBAC-dots**; (b) particle size distribution; (c) XPS full-scan spectrum of **PBAC-dots**; (d) IR spectrum of **PBAC-dots**.

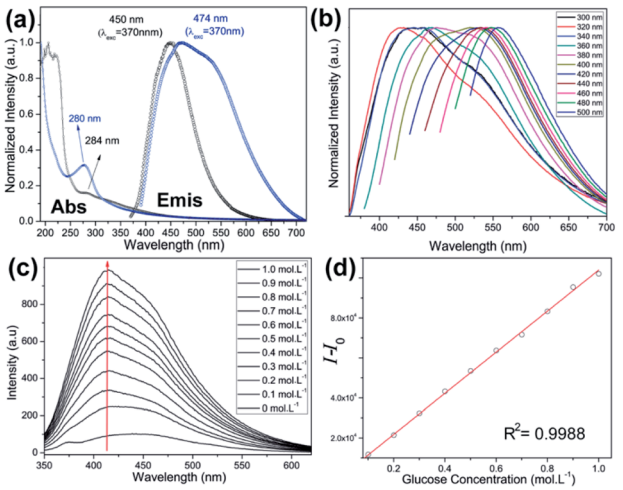

Fig. 2 (a) Absorption (Abs) and emission (Emis) spectra acquired at room temperature of **C-dot-NH$_2$** (black) and **PBAC-dots** (blue); (b) normalized emission spectra as function of excitation wavelength of **PBAC-dots**; (c) emission spectra as function of glucose concentration of **PBAC-dots**; (d) linear plot of integrated emission as function of glucose concentration. I_0 and I are the integrated emission spectra of **PBAC-dots** in absence and presence of the analyte.

–B–O groups, respectively. The N 1s peak centred at 402 eV (Fig. S1(c)†) may be attributed to $(C)_3$–N (sp^3). The B 1s spectra, displayed at Fig. S1(d),† show three peaks centred at 194.5, 191.7 and 188.3 eV, which are clearly ascribed to the B–O_2, B–O and B–C bonds, respectively. The infrared spectrum of the **PBAC-dots** (Fig. 1(d)) corroborates with the XPS spectroscopy analysis, since it shows characteristic peaks of B–O stretching vibration at 1378 cm^{-1}, B–O–H bending vibrations at 1160 and 1030 cm^{-1}, and C–B stretching at 1090 cm^{-1}.

Surface-engineering with functional ligands plays an important role endowing nanoparticles for biomedical applications, since these modifications can contribute to the improvement of their optical and magnetic properties, solvent affinity, biocompatibility and nontoxicity.[33] In addition, these functional surface agents corroborate for increasing the specificity, tuning the kinetics of the nanoparticles in biological environments, and enhancing colloidal stability. The optical properties of the C-dot are especially sensible to minimal surface modifications. Recent reports have confirmed that the presence of electron-donor or withdrawing groups, pH, solvent molecules, ions and surface defects, can perturb electronic structure over the nanoparticle surface.[34–36] Electronic effects of modified **PBAC-dots** were investigated by means of optical spectroscopy. The luminescent properties of the **PBAC-dots** are exhibited in Fig. 2.

The UV-Vis absorption spectra, measured for **C-dot-NH$_2$** and **PBAC-dots**, show bands centred at 280 and 284 nm, respectively. These absorptions are typical of n → π* transitions and provide evidence that the presence of withdrawing groups onto **PBAC-dots** surface slightly reduces the band gap energy.[32,37,38] The normalized emission spectra of the **C-dot-NH$_2$** and **PBAC-dots** acquired at room temperature with excitation at 360 nm, Fig. 2(a), exhibit maxima centred at 450 and 475 nm, respectively. These results suggest that the optical properties of **C-dot-NH$_2$** and **PBAC-dots** are not entirely controlled by the quantum confinement effect and the different behaviours can be attributed to the surface functionalization. The excitation-dependent emissions (Fig. 2(b)) suggest the presence of different emissive states onto **PBAC-dots** surface. Remarkably, this spectral behaviour has been widely reported for **C-dots** obtained from distinct carbon sources and synthetic methods. **C-dots** structure consists of a crystalline graphitic core covered by an amorphous carbon structure, which are embedded by heterogeneous population of fluorophores. These fluorophores can be responsible for the typical excitation-dependent emission spectra.[39]

Interest in boronic-acid-functionalized **C-dots** has soared in recent years concomitant to the huge evolution of glycobiology and its implications in treatments and diagnostics of severe pathologies. Production of boronic-containing **C-dots** is cheap, fast and can be rapidly performed in a unique step *via* hydrothermal or microwave synthesis. Several groups have produced and explored these optical probes as a non-enzymatic approach for saccharides detection in different environments.[40–43] Xu and co-workers obtained a boronic-containing optical probe for detection of sialic acid in aqueous solution, using the sole precursor 3-pyridylboronic acid in a one-step hydrothermal synthesis.[44] Phenylboronic acid and ethylenediamine were used to produce functionalized **C-dots** for detecting glycoproteins.[45] It is important to note that the examples mentioned above are selective, reproductive and presented good detection limits. However, in all cases, the probes responses are associated with luminescence quenching. This "turn-off" effect on C-dot emissions is not clear. Some studies have justified that quenching occurs due to particle aggregations.[42,45,46] Boron hybridization changes and/or the presence of nonradiative channels induced by electrostatic forces—aggregation/disaggregation caused by the anionic form of the boronic acid upon analyte complexation is another possible mechanism for the quenching.[47] The lack of knowledge on the mechanism of saccharide complexations and

© 2021 The Author(s). Published by the Royal Society of Chemistry

Open Access Article. Published on 03 ferraghju 2021. Downloaded on 30/07/2025 8:35:33.
This article is licensed under a Creative Commons Attribution-NonCommercial 3.0 Unported Licence.

how it affects luminescence indicates an open field for further investigations.

Usually, "light-down" probes might be inaccurate in sensing and might have limited work environment. On the other hand, "light-up" sensors are normally preferred due to their enhanced sensing capacity, especially in biological medium where the background fluorescence is highly problematic. Fig. 2(c) displays the emission intensity of **PBAC-dots** as a function of glucose concentration. Binding with glucose enhances emission intensities up to 6-fold relative to **PBAC-dots** and presents a good linear relationship ($R^2 = 0.998$) as shown in Fig. 2(d). The presence of an electron-donor group in the chemical structure of boronic acid derivatives is well-established as a cornerstone for the design of "light-up" sensors.[48,49] Therefore, the antagonist behaviour presented by **PBAC-dots** in presence of glucose does not arise from a simple accident or haphazard. In fact, this emerges from a previous stratagem used in boronic acid derivatives.[48–51] In general, surface functionalization of nanoparticles is one of the most important limiting factors for biomedical applications, because it affects the cytotoxic properties, the dynamic of cell uptake and selectivity.[52,53]

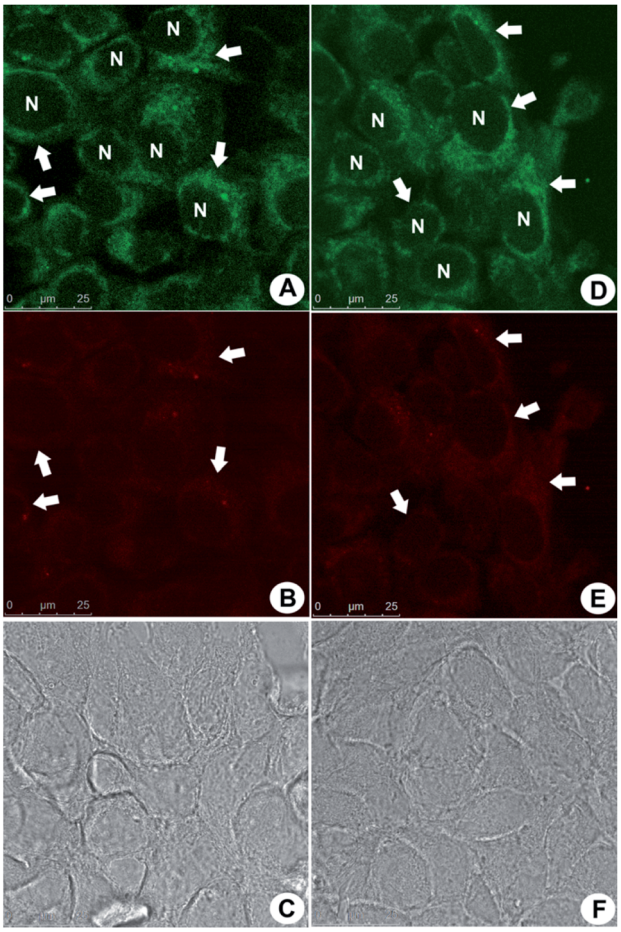

Fig. 3 MCF-7 breast cancer cells incubated with **PBAC-dots** and visualized on both the green and red channels. (A)–(C) Live cells. (D) and (E) Adhered cells. No staining could be detected inside the nuclei of the cells as shown by dark voids (N). (C) and (F) show the normal morphological aspects of the cells by phase contrast microscopy.

The performance of **PBAC-dots** probe in *in vitro* bioimaging experiments was also evaluated using MCF-7 cells (Fig. 3). **PBAC-dots** displayed an intense fluorescent signal in confocal microscope at both green and red channels. In addition, no cytotoxicity evidence was observed. MTT assays obtained also for other cell lines (Fig. S2†) showed no deleterious effect.

The fluorescent profile obtained in cells after **PBAC-dots** incubation indicates selective mitochondrial staining (Fig. 3). It is noteworthy to mention the fact that **PBAC-dots** were not found inside the nuclei of the cells, contrasting with previous results from **C-dots** passivated exclusively with ethylenediamine (**C-dot-NH$_2$**),[31] which were selective to nucleoli acid components inside the nuclei. Many works have depicted that **C-dots** are in general noncytotoxic and can be easily internalized by the cell.[54] However, Havrdova and co-workers demonstrated the toxicity-dependence of **C-dots** as function of surface charge.[55] In this study, negatively charged **C-dots** have shown almost no cytotoxicity for high concentrations (0.1 mg mL^{-1}). Cytotoxicity of **PBAC-dots** on melanoma (B16F10) and fibroblast (NIH3T3) murine cells was evaluated in three different concentrations (0.01, 0.05 and 0.1 mg mL^{-1}) during 24 h, and afterwards MTT assays were performed to evaluate the cell viability. The only concentration that showed significant toxicity was 0.1 mg mL^{-1} for B16F10 and NIH3T3 cells ($p < 0.01$). The apparent low

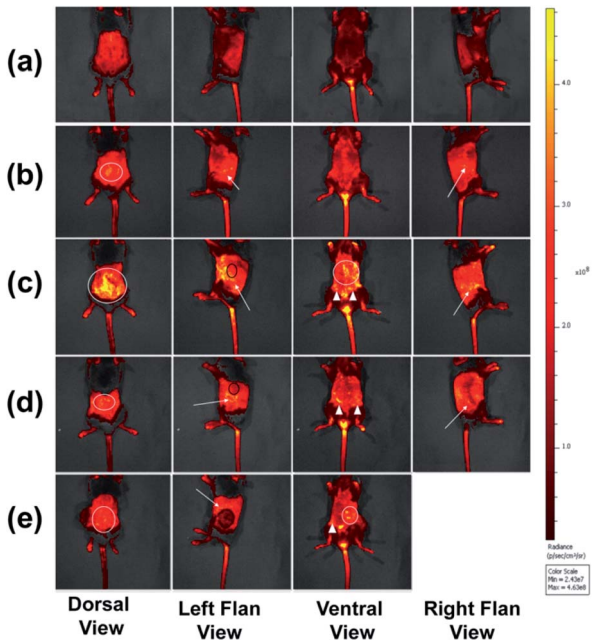

Fig. 4 Representative *in vivo* fluorescence bioimaging for anesthetized C57BL/6 mice (a) control; (b) non-tumour mice acquired 4 h after administration of **PBAC-dots** (0.16 mg mL^{-1}); (c) melanoma-bearing mice 4 days after tumour induction and 4 h after administration of **PBAC-dots** (0.16 mg mL^{-1}); (d) melanoma-bearing mice 8 days after tumour induction and 4 h after administration of **PBAC-dots** (0.16 mg mL^{-1}); (e) melanoma-bearing mice 14 days after tumour induction and 4 h after administration of **PBAC-dots** (0.16 mg mL^{-1}). White circles indicate fluorescence on dorsal regions. White arrows emphasize fluorescence on the kidney region. White triangles indicate the fluorescence in ureter regions and black circles indicate the tumour region.

© 2021 The Author(s). Published by the Royal Society of Chemistry

Open Access Article. Published on 03 ferraghju 2021. Downloaded on 30/07/2025 8:35:33.
This article is licensed under a Creative Commons Attribution-NonCommercial 3.0 Unported Licence.

cytotoxicity of **PBAC-dots** can be justified by the presence of negative surface charges centred at boronic groups at physiological pH.[56]

The "light-up" characteristic of **PBAC-dots** and the high complexing affinity at pH 7.4 between the boronic and sialic acid groups open up the opportunity to explore this nanoprobe as a tumour imaging agent using *in vivo* models.[18,56] It is well-known that melanoma murine B16F10 cells are tremendously aggressive, can metastasize from a primary subcutaneous site to the lungs and present high levels of sialic acid expressed on their membrane.[57] Hence, to validate the feasibility of the *in vivo* bioimaging probe, experiments on skin cancer-bearing mice were conducted. All animal procedures were performed in accordance with the Guidelines for Care and Use of Laboratory Animals of University of Brasilia (UnB) and experiments were approved by the Animal Ethics Committee of UnB. The subcutaneous injection of 10^5 B16F10 cells resulted in tumour growth at the injection site. Fluorescence bioimaging of C57BL/6 mice can be seen in Fig. 4.

All C57BL/6 mice treated with **PBAC-dots** presented several fluorescent spots spread all along animal bodies. The bioimaging of healthy C57BL/6 mice treated with **PBAC-dots** was used as control as shown in Fig. 4(a). It was possible to observe the fluorescence on the kidneys and ureter regions, which is a clear indication of the **PBAC-dots** excretion *via* the urinary system. Licciardello and co-workers found that carbon quantum dots had been mainly eliminated by kidneys after 60 minutes of their application.[58] The histological studies demonstrated no abnormalities on brain, kidney, spleen, lung and liver tissues, such as necrosis, apoptosis or haemorrhage (see Fig. 5(b)). Haematological and serum biochemistry assays are in good agreement with the histological result since they did not show evidence of toxicological disturbances in healthy mice treated with **PBAC-dots** (Fig. S28–S30†).

The bioimages of the cancer-bearing mice acquired 4 h after **PBAC-dots** administration (0.16 mg mL^{-1}), Fig. 4(c)–(e), show a dispersive fluorescent pattern suggesting that the probe is not selective to the tumour region. Other *in vivo* fluorescent images acquired after 2, 6, 24 and 48 h of 0.16 and 0.32 mg mL^{-1} administrations of **PBAC-dots** presented the same behaviour and are available in Fig. S3–S26.† It was possible to observe luminescent spots on kidney and ureter regions.

The histopathological images of the organs are shown in Fig. 5. The studies demonstrated no evidence of tissue damage on the brain and kidneys for all cancer-bearing mice treated with **PBAC-dots**, whereas inflammatory focus and white pulp hyperplasia were observed in liver and spleen tissues, respectively. On lung tissue, there are areas of fibrosis and inflammatory infiltrate.

Fig. 6 shows the histological analysis of the tumour tissues. Surprisingly, after the treatment with **PBAC-dots** a large number of areas of necrosis and inflammatory infiltrate were revealed, which were not identified for cancer-bearing mice without the treatment (Fig. 6(b)–(d)).

Similar results were reported when **C-dots** and graphene-oxide were used in photodynamic therapy,[59,60] however, **PBAC-dots** were able to introduce tumour lesion without external stimulus. Haematological assays were also used to shed light on this astonishing therapeutic effect of the **PBAC-dots**. The major haematological parameters are similar to those presented by the control group, except for the number of white blood cells in cancer-bearing mice whose blood samples were collected 30 days after **PBAC-dots** administration. This alteration can be interpreted as a response of immunological system for the

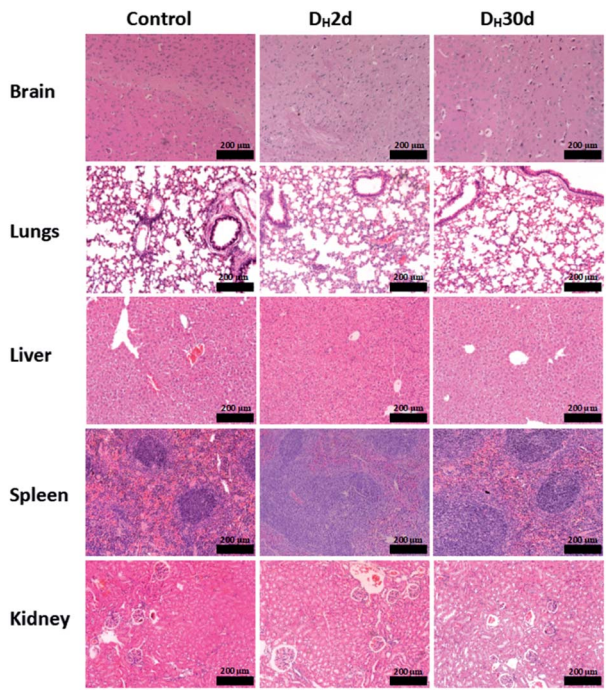

Fig. 5 Histological images of the brains, lungs, livers, spleens and kidneys of the control and cancer-bearing mice treated with **PBAC-dots**.

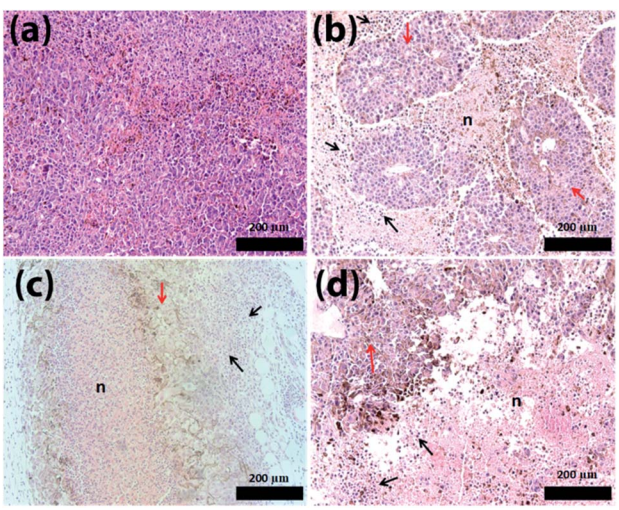

Fig. 6 Histological images of the tumour. (a) Cancer-bearing mice without **PBAC-dots** treatment. Histological images of the tumour-bearing mice treated 0.16 mg mL^{-1} of **PBAC-dots** after 4 (b), 8 (c) and 14 (d) days of cancer induction. The "n' indicates necrosis regions, red and black arrows indicate intact tumoral tissue and Immunological cells, respectively.

© 2021 The Author(s). Published by the Royal Society of Chemistry

Open Access Article. Published on 03 ferraghju 2021. Downloaded on 30/07/2025 8:35:33.
This article is licensed under a Creative Commons Attribution-NonCommercial 3.0 Unported Licence.

higher cancer stage, since previous reports have demonstrated that **C-dots** presented non toxicological effects on haematological parameters after 28 days of treatment.[60] Lymphogram results showed a growth of lymphocyte percentage for cancer-bearing mice euthanized 2 and 30 days after treatment, (Fig. S28†). Therefore, **PBAC-dots** can either interact with the tumour and stimulate the immune system to respond more strongly against the disease, or can interfere indirectly on cancer cells abilities to keep themselves undetectable by the immune system.[61] Both hypotheses are plausible for explaining the lesion on the tumour.

Bortezomib (Velcade) is a kind of dipeptide boronic acid that acts as a proteasome inhibitor and was approved by the U.S. Food and Drug Administration (FDA) for use in therapies for a myriad of cancers. The boronic group of the Bortezomib is associated with the protease inhibition that contributes to sensitizing solid tumours to T-cell-mediated killing, stabilizing T-cell activation, and thus improving the outcome of adoptive T-cell therapy of cancer.[62–65] Tumour cells are apparently more susceptible to proteasome inhibition than normal cells caused by the loss of checkpoint mechanisms that occurs during tumorigenesis. Bortezomib and **PBAC-dots** have the boronic acid group incorporated in their structures, thus allowing us to highlight the importance of this acid to the observed outcomes. The results presented in this work also indicate the potential of **PBAC-dots** as checkpoint inhibitor.

Mechanistic knowledge of the cancer sensitization induced by **PBAC-dots** is vital for expanding its application in different cancers and pathologies, however, for that, it would be required more specific studies on a molecular level base.

Conclusions

In summary, it was demonstrated that the strategy adopted to modify the **C-dots** surface with PBA moieties resulted in a nontoxic light-up probe for glucose detection in aqueous solution, that was well tolerated by mice. It was also determined that **PBAC-dots** can induce necrosis in tumour tissues in cancer-bearing mice. Cell imaging experiments indicated the preference for mitochondria and it could be visualized in both green and red channels. The haematological studies showed a significative increase of lymphocyte that can be associated with immunological stimulation. Future works will be focused on elucidating the antitumoral mechanism of **PBAC-dots**.

Author contributions

These authors contributed equally.

Conflicts of interest

There are no conflicts to declare.

Acknowledgements

The authors gratefully acknowledge CNPq, CAPES, DPG-UnB, FAP-DF, LNLS, Sabin Institute and Labmic for their support. This work is in memory of the student Christian Lima Costa Vasconcelos.

References

1 F. Bray, J. Ferlay, I. Soerjomataram, R. L. Siegel, L. A. Torre and A. Jemal, *Ca-Cancer J. Clin.*, 2018, **68**, 394–424.
2 W. Fan, B. Yung, P. Huang and X. Chen, *Chem. Rev.*, 2017, **117**, 13566–13638.
3 V. Labhasetwar, M. Zborowski, A. R. Abramson and J. P. Basilion, *Mol. Pharmaceutics*, 2009, **6**, 1261–1262.
4 S. Siddique and J. C. Chow, *Nanomaterials*, 2020, **10**, 1700.
5 J. P. António, R. Russo, C. P. Carvalho, P. M. Cal and P. M. Gois, *Chem. Soc. Rev.*, 2019, **48**, 3513–3536.
6 M. Lei, H. Feng, E. Bai, H. Zhou, J. Wang, Y. Qin, H. Zhang, X. Wang, Z. Liu and O. Hai, *Org. Biomol. Chem.*, 2019, **17**, 683–691.
7 P. C. Trippier and C. McGuigan, *MedChemComm*, 2010, **1**, 183–198.
8 A. E. Pasqua, B. Wilding, M. Cheeseman and K. Jones, *J. Med. Chem.*, 2017, **60**, 180–201.
9 A. C. Li, E. Yu, S. C. Ring and J. P. Chovan, *Chem. Res. Toxicol.*, 2013, **26**, 608–615.
10 J. M. Seeger, P. Schmidt, K. Brinkmann, A. A. Hombach, O. Coutelle, P. Zigrino, D. Wagner-Stippich, C. Mauch, H. Abken and M. Krönke, *Cancer Res.*, 2010, **70**, 1825–1834.
11 C.-J. Lu, J. Hu, Z. Wang, S. Xie, T. Pan, L. Huang and X. Li, *MedChemComm*, 2018, **9**, 1862–1870.
12 M. Marasovic, S. Ivankovic, R. Stojkovic, D. Djermic, B. Galic and M. Milos, *J. Enzyme Inhib. Med. Chem.*, 2017, **32**, 1299–1304.
13 S. Deshayes, H. Cabral, T. Ishii, Y. Miura, S. Kobayashi, T. Yamashita, A. Matsumoto, Y. Miyahara, N. Nishiyama and K. Kataoka, *J. Am. Chem. Soc.*, 2013, **135**, 15501–15507.
14 H. Einsele, in *Small Molecules in Oncology*, Springer, 2014, pp. 325–345.
15 E. M. McAuley, T. A. Bradke and G. E. Plopper, *Cell Adhes. Migr.*, 2011, **5**, 382–386.
16 X. Wang, H. Tang, C. Wang, J. Zhang, W. Wu and X. Jiang, *Theranostics*, 2016, **6**, 1378.
17 J. Wang, W. Wu and X. Jiang, *Nanomedicine*, 2015, **10**, 1149–1163.
18 H. Liu, Y. Li, K. Sun, J. Fan, P. Zhang, J. Meng, S. Wang and L. Jiang, *J. Am. Chem. Soc.*, 2013, **135**, 7603–7609.
19 S. S. Pinho and C. A. Reis, *Nat. Rev. Cancer*, 2015, **15**, 540–555.
20 I. Häuselmann and L. Borsig, *Front. Oncol.*, 2014, **4**, 28.
21 A. V. D. Lazescu, R. M. Anghel and D. A. Galvan, *Rom. Rev. Lab. Med.*, 2014, **21**, 179–188.
22 A. V. D. Lazescu, M. I. I. Gruia, R. M. Anghel and D. A. Glavan, *Rev. Rom. Med. Lab.*, 2013, **21**, 179–188.
23 T. M. Bradke, C. Hall, S. W. Carper and G. E. Plopper, *Cell Adhes. Migr.*, 2008, **2**, 153–160.
24 A. Kim, M. Suzuki, Y. Matsumoto, N. Fukumitsu and Y. Nagasaki, *Biomaterials*, 2020, **268**, 120551.
25 K. Hola, Y. Zhang, Y. Wang, E. P. Giannelis, R. Zboril and A. L. Rogach, *Nano Today*, 2014, **9**, 590–603.

Open Access Article. Published on 03 ferraghju 2021. Downloaded on 30/07/2025 8:35:33.
This article is licensed under a Creative Commons Attribution-NonCommercial 3.0 Unported Licence.

26 D. Qu and Z. Sun, *Mater. Chem. Front.*, 2020, **4**, 400–420.
27 D. Qu, X. Wang, Y. Bao and Z. Sun, *J. Phys.: Mater.*, 2020, **3**, 022003.
28 Q. Jia, Z. Zhao, K. Liang, F. Nan, Y. Li, J. Wang, J. Ge and P. Wang, *Mater. Chem. Front.*, 2020, **4**, 449–471.
29 M. Fahmi, W. Sukmayani, S. Q. Khairunisa, A. Witaningrum, D. Indriati, M. Matondang, J.-Y. Chang, T. Kotaki and M. Kameoka, *RSC Adv.*, 2016, **6**, 92996–93002.
30 M. Z. Fahmi, J.-K. Chen, C.-C. Huang, Y.-C. Ling and J.-Y. Chang, *J. Mater. Chem. B*, 2015, **3**, 5532–5543.
31 C. D'Angelis do ES Barbosa, J. R. Corrêa, G. A. Medeiros, G. Barreto, K. G. Magalhães, A. L. de Oliveira, J. Spencer, M. O. Rodrigues and B. Amaro Neto, *Chem.–Eur. J.*, 2015, **21**, 5055–5060.
32 J. Ge, Q. Jia, W. Liu, M. Lan, B. Zhou, L. Guo, H. Zhou, H. Zhang, Y. Wang and Y. Gu, *Adv. Healthcare Mater.*, 2016, **5**, 665–675.
33 R. A. Petros and J. M. DeSimone, *Nat. Rev. Drug Discovery*, 2010, **9**, 615–627.
34 S. Dutta Choudhury, J. M. Chethodil, P. M. Gharat, P. K. Praseetha and H. Pal, *J. Phys. Chem. Lett.*, 2017, **8**, 1389–1395.
35 X. Li, S. Zhang, S. A. Kulinich, Y. Liu and H. Zeng, *Sci. Rep.*, 2014, **4**, 4976.
36 C. Ding, A. Zhu and Y. Tian, *Acc. Chem. Res.*, 2014, **47**, 20–30.
37 W. Kwon, G. Lee, S. Do, T. Joo and S. W. Rhee, *Small*, 2014, **10**, 506–513.
38 Q. Hu, M. C. Paau, Y. Zhang, W. Chan, X. Gong, L. Zhang and M. M. Choi, *J. Chromatogr. A*, 2013, **1304**, 234–240.
39 S. Divya, S. Narayan, S. R. K. Ainavarapu and D. Khushalani, *ChemPhysChem*, 2019, **20**, 984–990.
40 P. Shen and Y. Xia, *Anal. Chem.*, 2014, **86**, 5323–5329.
41 M.-J. Cho and S.-Y. Park, *Sens. Actuators, B*, 2019, **282**, 719–729.
42 W.-S. Zou, C.-H. Ye, Y.-Q. Wang, W.-H. Li and X.-H. Huang, *Sens. Actuators, B*, 2018, **271**, 54–63.
43 S. Kiran and R. Misra, *J. Biomed. Mater. Res., Part A*, 2015, **103**, 2888–2897.
44 S. Xu, S. Che, P. Ma, F. Zhang, L. Xu, X. Liu, X. Wang, D. Song and Y. Sun, *Talanta*, 2019, **197**, 548–552.
45 X. Zhang, L. Chai, S. Nie, C. Lv, Q. Wang and Z. Li, *Analyst*, 2019, **144**, 1975–1981.
46 A. S. Krishna, P. A. Nair, C. Radhakumary and K. Sreenivasan, *Mater. Res. Express*, 2016, **3**, 055001.
47 Z.-b. Qu, X. Zhou, L. Gu, R. Lan, D. Sun, D. Yu and G. Shi, *Chem. Commun.*, 2013, **49**, 9830–9832.
48 X. Sun, T. D. James and E. V. Anslyn, *J. Am. Chem. Soc.*, 2018, **140**, 2348–2354.
49 N. DiCesare and J. R. Lakowicz, *J. Phys. Chem. A*, 2001, **105**, 6834–6840.
50 T. D. James, K. S. Sandanayake, R. Iguchi and S. Shinkai, *J. Am. Chem. Soc.*, 1995, **117**, 8982–8987.
51 X. Liu, X. Hu, Z. Xie, P. Chen, X. Sun, J. Yan and S. Zhou, *Anal. Methods*, 2016, **8**, 3236–3241.
52 P. Patel, A. Hanini, A. Shah, D. Patel, S. Patel, P. Bhatt and Y. V. Pathak, in *Surface Modification of Nanoparticles for Targeted Drug Delivery*, Springer, 2019, pp. 19–31.
53 S. Salatin, S. Maleki Dizaj and A. Yari Khosroushahi, *Cell Biol. Int.*, 2015, **39**, 881–890.
54 K. Ghosal and A. Ghosh, *Mater. Sci. Eng. C*, 2019, **96**, 887–903.
55 M. Havrdova, K. Hola, J. Skopalik, K. Tomankova, M. Petr, K. Cepe, K. Polakova, J. Tucek, A. B. Bourlinos and R. Zboril, *Carbon*, 2016, **99**, 238–248.
56 H. Otsuka, E. Uchimura, H. Koshino, T. Okano and K. Kataoka, *J. Am. Chem. Soc.*, 2003, **125**, 3493–3502.
57 Y. Long, Z. Lu, L. Mei, M. Li, K. Ren, X. Wang, J. Tang, Z. Zhang and Q. He, *Adv. Sci.*, 2018, **5**, 1800229.
58 N. Licciardello, S. Hunoldt, R. Bergmann, G. Singh, C. Mamat, A. Faramus, J. L. Ddungu, S. Silvestrini, M. Maggini and L. De Cola, *Nanoscale*, 2018, **10**, 9880–9891.
59 S. Beack, W. H. Kong, H. S. Jung, I. H. Do, S. Han, H. Kim, K. S. Kim, S. H. Yun and S. K. Hahn, *Acta Biomater.*, 2015, **26**, 295–305.
60 J. Ge, M. Lan, B. Zhou, W. Liu, L. Guo, H. Wang, Q. Jia, G. Niu, X. Huang and H. Zhou, *Nat. Commun.*, 2014, **5**, 1–8.
61 M. S. Goldberg, *Cell*, 2015, **161**, 201–204.
62 A. Shanker, S. T. Pellom, D. F. Dudimah, M. C. Thounaojam, R. L. De Kluyver, A. D. Brooks, H. Yagita, D. W. McVicar, W. J. Murphy and D. L. Longo, *Cancer Res.*, 2015, **75**, 5260–5272.
63 S. T. Pellom Jr, D. F. Dudimah, M. C. Thounaojam, R. V. Uzhachenko, A. Singhal, A. Richmond and A. Shanker, *Oncotarget*, 2017, **8**, 8604.
64 J.-E. Kim, D.-H. Jin, W. J. Lee, D. Hur, T.-C. Wu and D. Kim, *Pharmacol. Res.*, 2013, **71**, 23–33.
65 S. T. Pellom Jr, D. F. Dudimah, M. C. Thounaojam, T. J. Sayers and A. Shanker, *Immunotherapy*, 2015, **7**, 1011–1022.

© 2021 The Author(s). Published by the Royal Society of Chemistry